Journal of Materials Chemistry A

Accepted Manuscript

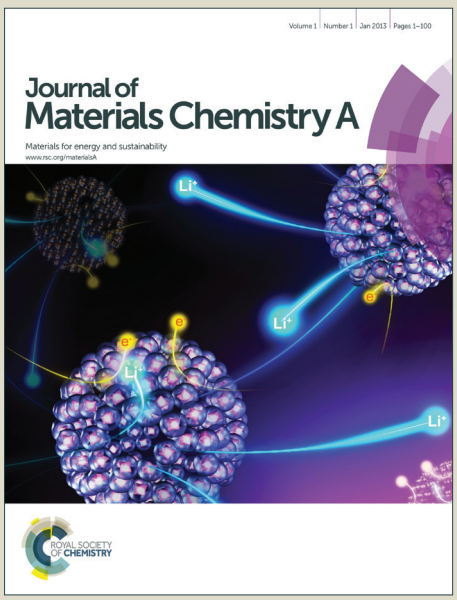

ROYAL SOCIETY OF CHEMISTRY

www.rsc.org/materialsA

Journal Name

RSCPublishing

ARTICLE

Electrochemically grown three-dimensional porous Si@Ni inverse opal structure for higher-performance Li ion battery anode

Do Youb Kim,[a] Jungdon Suk,[a] Dong Wook Kim,[a] Yongku Kang,*[a] Sang Hyuk Im,[b] Youngjo Yang,[c] O Ok Park[c]

Cite this: DOI: 10.1039/x0xx00000x

Received 00th January 2012,
Accepted 00th January 2012

DOI: 10.1039/x0xx00000x

www.rsc.org/

We report a facile method for the fabrication of a three-dimensional (3D) porous silicon@nickel (Si@Ni) inverse opal structure for Li ion batteries by using an electrodeposition method and a colloidal crystal as a sacrificial template. The Ni inverse opal structure was fabricated first by electrodeposition of Ni on the pre-formed colloidal crystal template, followed by removal of the template. Finally, the Si@Ni inverse opal structure was obtained by electrodeposition of Si onto the Ni inverse opal structure. The highly porous structure of the electrode containing a conductive and mechanically strong Ni scaffold could sufficiently accommodate volume expansion during the Si–Li alloying. A coin cell using the Si@Ni inverse opal structure as an anode exhibited a high charge capacity of 2548.5 mAh g^{-1}, stable cycling retention, and high rate performance without the need for a binder or conducting additives.

Introduction

Lithium (Li) ion batteries (LIBs) are currently one of the most important energy storage systems. They are considered to be promising candidates for numerous applications such as several kinds of electric vehicles, portable electronics, and microelectronic devices because of their high energy density and efficiency, lack of memory effect, long cycle life, and light weight, and because they are environmentally benign.[1-6] Because the demand for LIBs with higher performance has been increasing dramatically, tremendous efforts have been made to develop LIBs with higher capacity, longer cycle life, and faster charging rates.[7-15] As an anode material for higher-capacity LIBs, Si in particular has attracted much attention due to its high theoretical capacity (4200 mAh g^{-1}),[12,16] which is the highest known and much higher than that of currently used graphite-based anodes (372 mAh g^{-1}).[17] Nevertheless, Si has relatively low electron conductivity and Li ion diffusivity. More importantly, conventional Si anodes usually suffer from poor capacity retention due to a huge volume expansion (~400%) during alloying/dealloying with Li. Repeated volume expansion/contraction upon cycling leads to pulverization of electrodes.[18-20]

In order to solve the pulverization problem of a typical Si anode, there have been enormous efforts in give the available space within the electrode for accommodating Si volume change. For example, one-dimensional (1D) Si nanostructures such as nanowires and nanotubes grown by vacuum deposition methods have been fabricated for high-performance LIB anodes.[21-26] Other approaches have been based on the use of three-dimensional (3D) porous Si structures as anodes, where the porous Si structures were fabricated by etching bulk Si or vacuum deposition of Si onto 3D porous templates.[27-33] Although these Si nanostructures could exhibit high capacities, stable capacity retention, and good rate performance, most of the fabrication methods for these Si structures require relatively expensive equipment, disposal of etched Si, or heat treatment at relatively high temperatures.

Electrodeposition, where metal ions in an electrolyte are reduced by electrons provided by an external power supply, is an effective way to fabricate metal structures, and thus it has been widely used in many research fields and various industries. There are several advantages to using the electrodeposition method for fabricating metal structures: *i*) It is cost effective because it requires relatively inexpensive equipment and it enables a metal layer to be deposited on a relatively large substrate, *ii*) various metals and metal alloys can be deposited on a substrate, *iii*) the properties of the deposited layer can be varied by changing the composition of the electrolytes and additives, *iv*) the thickness and mass of the deposited layer can be easily controlled by using Faraday's laws of electrolysis, and *v*) deposition can be applied on substrates with complex architectures.[34-38]

Recently, we reported a facile method for the fabrication of 3D porous Si/Cu film for high-performance LIB anode by an electrodeposition using a hydrogen bubble template.[39] Hydrogen bubbles generated during Cu electrodeposition served as a dynamic template for the 3D porous Cu film with relatively large pores ranging from 30 to 80 μm. Although the 3D porous Si/Cu film showed excellent performance as a LIB anode, the fabrication method was still less capable of fabricating highly ordered structure with relatively small pores. As an extension of these results, in this study, we demonstrate the fabrication method for an electrochemically grown 3D porous Si@Ni inverse opal structure for high-performance LIB anodes. Both Ni and Si were electrodeposited using polystyrene (PS) colloidal crystals as a sacrificial template. By using PS colloidal crystals as a template, we could prepare highly ordered porous Ni structure. A 3D porous Ni scaffold could provide mechanical strength and electron conductivity to an anode. The 3D porous structure anode could also accommodate Si expansion during the alloying with Li and provide a high surface area and diffusion pathways for Li ions. Owing to these advantages, a coin-type cell using the 3D porous Si@Ni inverse opal structure as the anode exhibited a highly reversible charge capacity of 2458.4 mAh g^{-1}, 72.1% capacity retention after 100 cycles, and good rate performance even at 10 C.

Experimental

Materials

A styrene monomer (Aldrich), sodium styrene sulfonate (Aldrich), potassium persulfate (Aldrich), poly(vinylpyrrolidone) (PVP, Aldrich, Mw = 55,000), nickel sulfate (Aldrich), nickel chloride (Junsei), boronic acid (Aldrich), sodium dodecyl sulfate (SDS, Junsei), propylene carbonate (PC, Aldrich), silicon tetrachloride ($SiCl_4$, Aldrich), and tetrabutylammonium chloride (TBACl, Aldrich) were purchased and used as received. In all experiments, we used deionized (DI) water with a resistivity of 18.2 MΩ, which was prepared using a Milli-Q ultrapure water system (Millipore).

Preparation of 3D colloidal crystal template

PS colloidal particles with a diameter of 370 nm were prepared by emulsifier-free emulsion polymerization[40] and 3D PS colloidal crystal templates were fabricated using a convective self-assembly method.[41] For the conductive substrates, chromium (5 nm) as an adhesion layer and then gold (70 nm) were thermally evaporated on thoroughly cleaned slide glass. Then, the substrates were treated with piranha solution (H_2SO_4:H_2O_2 = 3:1, v/v) in order to create a hydrophilic substrate surface. For the fabrication of the coin cell, copper foil with a thickness of 25 μm (99.8%, Alfa Aesar) was used as a conductive substrate for fabricating the 3D PS colloidal crystals. The Cu foil was cleaned and treated with 0.1 M H_2SO_4 aqueous solution, isopropanol, and acetone in order before use. To assemble the 3D colloidal crystals, the substrates were dipped into a 0.1 wt% PS colloidal suspension (40 mL) containing 0.1 mL of PVP aqueous solution (0.5 wt%). Then, the colloidal suspensions were dried in an oven at 63 °C until completely dry. To enhance the connection strength between the PS colloidal particles and between the PS colloidal crystals and the substrates, the samples were annealed at 95 °C for 5 h.

Electrodeposition of Ni

The Ni electrodeposition solution was prepared by dissolving nickel sulfate (50 g), nickel chloride (12 g), boronic acid (8 g), and SDS (1 g) in DI water (200 mL). The substrate with the 3D PS colloidal template was assembled into a home-made cell made with Teflon™. Using a pure nickel plate as the counter electrode, nickel was electrodeposited into the 3D PS colloidal template on a conductive substrate at a current density of 0.4 mA cm^{-2} for 5000 s. After completion of the electrodeposition, the sample was rinsed with DI water and the PS colloidal template was dissolved with tetrahydrofuran.

Electrodeposition of Si

Electrodeposition of Si was performed in a Ar-filled glove box with a PC solution containing TBACl (0.1 M) and $SiCl_4$ (0.1 M).[42,43] The Si electrodeposition was carried out in a three-electrode system consisting of Pt mesh and Ag wire as the counter and reference electrodes, respectively. Si was electrodeposited into the 3D inverse opal structure of Ni at −2.0 V for 1700 s and then the substrate was rinsed with pure PC several times.

Characterization

SEM images were obtained using a field-emission scanning electron microscope (Mira III, Tescan) equipped with an energy dispersive X-ray spectrometer (EDS) and operated at an accelerating voltage of 10–20 kV. XPS analysis was performed with an Omicron ESCA probe spectrometer using a monochromatic (Al Kα, 1486.6 eV) source. The electrochemical performance of the 3D porous Si@Ni inverse opal structure anode was tested in a coin-type half-cell that was fabricated in an Ar-filled glove box using Li metal as the counter electrode and Celgard 2400 as a separator. A binder

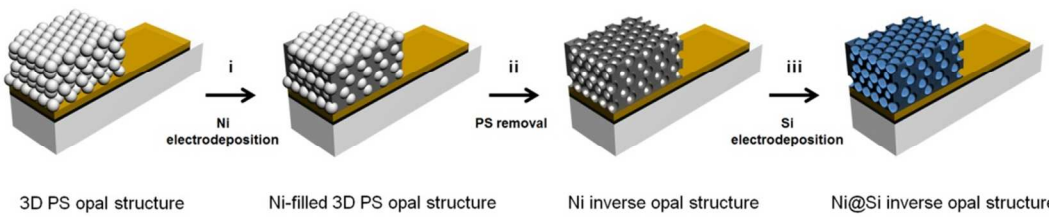

Fig. 1 Schematic illustration of the fabrication procedure for the 3D Si@Ni inverse opal structure.

and conducting additives were not used. As an electrolyte, 1.0 M $LiPF_6$ in 1:1 w/w ethylene carbonate/propylene carbonate (Soulbrain, Korea) was used. All measurements were conducted using a VMP3 potentiostat (BioLogic, France). CV tests were conducted in the voltage range between 0.01–2.0 V *vs*. Li/Li^+ at a scan rate of 0.1 mV s^{-1} and galvanostatic cycling was tested in the same voltage range

Results and discussion

Fig. 1 shows the fabrication procedure for the 3D porous Si@Ni inverse opal structure (see the experimental section for detailed experimental procedure). First, a 3D opal structure of PS colloidal particles was fabricated on a conducting substrate by the convective self-assembly method.[41] As seen in Fig. 2A, a 3D opal structure of PS colloidal particles with a diameter of *ca*. 370 nm was well fabricated on a Cr/Au-coated slide glass. The thickness of the structure was measured to be *ca*. 7.5 μm (inset in Fig. 2A). This 3D PS opal structure was then heated at 95 °C for 5 h to enhance the adhesion between the PS colloidal particles themselves and between the particles and the substrate. Then, the PS 3D opal structure served as a sacrificial template for preparing the inverse opal structure of the Ni current collector scaffold. The Ni inverse opal structure was fabricated by using an electrodeposition technique through the 3D PS opal, with a pure Ni plate as the counter electrode in the Ni electroplating solution, followed by removal of the PS with tetrahydrofuran. Fig. 2B shows the top-view SEM image of the 3D Ni inverse opal structure, which was electrodeposited at a current density of 0.4 mA cm^{-2} for 5000 s. The figure shows the well-ordered and highly porous 3D inverse opal structure of Ni.

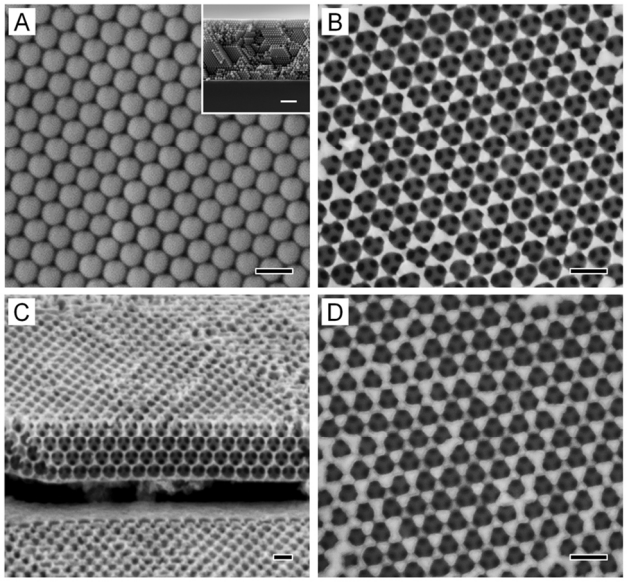

Fig. 2 SEM images of different structures obtained at each fabrication stage on Cr/Au-coated slide glass substrates. (A) Top-view and cross-sectional view (inset) images of 3D PS opal structure, (B) top-view image of Ni inverse opal structure after Ni electrodeposition and removal of PS template, (C) tilted-view image of Ni inverse opal structure, and (D) top-view image of Si-deposited Ni inverse opal structure. The scale bars represent 500 nm (inset: 2 μm).

Fig. 2C shows a tilted-view SEM image of a broken part of the Ni inverse opal structure. The structure is completely open, with pores from the bottom to the top surfaces and a thickness of *ca*. 1.5 μm. Finally, Si was electrodeposited on the 3D inverse opal structure of the Ni current collector scaffold. Fig. 2D shows a top-view SEM image of the structure after Si electrodeposition at the constant potential of −2.0 V for 1700 s. As compared to the Ni inverse opal structure shown in Fig. 2B (with the same magnification), the 3D porous Si@Ni structure exhibited a slightly smaller pore size and a light-colored layer with a thickness of *ca*. 30 nm on Ni scaffolds, indicating that Si was well electrodeposited on the Ni inverse opal structure.

We then expanded the fabrication of the 3D Si@Ni inverse opal structure onto a Cu foil in order to use the structure as an electrode for a coin-type battery for stable electrochemical characterization. Although the regularity of the PS particles, and thus the pores in the Ni inverse opal structure, was slightly lower than that of the structures fabricated on the Cr/Au-coated

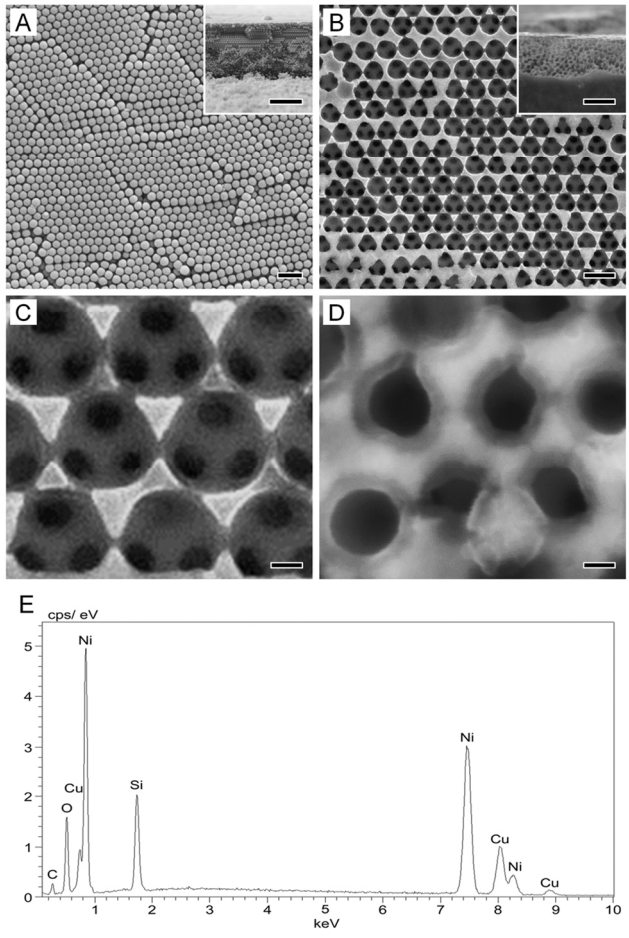

Fig. 3 SEM images of different structures obtained at each fabrication stage on Cu foil substrates. (A) Top-view and cross-sectional view (inset) images of 3D PS opal structure, (B) top-view and cross-sectional view (inset) images of Ni inverse opal structure after Ni electrodeposition and removal of PS template, (C) higher magnification image of Ni inverse opal structure, and (D) Si-deposited Ni inverse opal structure. Scale bars represent (A) 1 μm (inset: 5 μm), (B) 500 nm (inset: 2 μm), and (C and D) 100 nm. (E) EDS spectrum of the Si@Ni inverse opal structure fabricated on a Cu foil substrate.

slide glass due to the higher roughness of the Cu foil surface, the 3D PS opal structure and Ni inverse opal structure were successfully fabricated on the Cu foil (Fig. 3A and 3B). The thicknesses of the PS colloidal crystal and Ni inverse opal structures were measured to be *ca*. 9 μm and *ca*. 2 μm, respectively (insets in Fig. 3A and 3B). Fig. 3C and 3D show high-magnification SEM images (with the same magnification) of the 3D Ni inverse opal structures before and after Si electrodeposition, respectively, for better comparison. A thin layer of Si was successfully electrodeposited on the Ni inverse opal surface with a thickness of *ca*. 50 nm. The discrepancy between the thickness of the Si layer on the Cr/Au-coated slide glass and that on the Cu foil was attributed to the lower regularity of the Ni inverse opal structure on the Cu foil and the different electron conductivities of the substrates used. The electrodeposited Si was also characterized by energy dispersive X-ray spectroscopy (EDS), which confirmed that the light-colored layer on the Ni inverse opal structure was Si with a few carbon impurities (Fig. 3E). These impurities were derived from the TBACl used as an additive for enhancing the conductivity of the electrolyte for Si electrodeposition.[42,43] The oxygen was likely derived from the air exposure of the sample for the analyses. Taking these results together, we can conclude that a 3D inverse opal structure of Si@Ni was well fabricated by the electrodeposition method on conducting substrates.

The electrochemical properties of the 3D porous Si@Ni inverse opal structure were characterized in a coin-type half-cell using Li foil as both the counter and reference electrodes. Fig. 4A shows the cyclic voltammetry (CV) curves of the Si@Ni inverse opal structure electrode for the first five cycles in the range between 0.01–2.0 V at a scan rate of 0.1 mV s^{-1}. The CV curves show reduction and oxidation peaks at potentials typical of the reaction of Si with Li,[31-33,44] indicating the reversible lithiation and delithiation reaction of the Si@Ni inverse opal structure electrode. During the first discharge, the broad and weak reduction peak at approximately 1.1 V could be attributed to side reactions of impurities on the Si surface, which were possibly generated during electrodeposition of Si and/or Ni, such as C and Cl from the electrolyte components.[42,43] Although the percentage of Cl was too low to be detected by EDS characterization, a Cl 2p peak was clearly visible in the XPS spectrum [Fig. S1† in the Electronic Supplementary Information (ESI)]. According to the XPS analysis, 29.5 at% of C and 4.9 at% of Cl were detected on the electrodeposited Si surface.

Fig. 4B shows the voltage profiles for the first four charge/discharge cycles recorded at a 0.05 C rate (1 C = 4.2 A g^{-1}). The gravimetric capacity of the 3D porous Si@Ni inverse opal structure was calculated based on the average mass of the electrodeposited Si. Note that in a previous report on the electrodeposition of Si using similar experimental conditions,

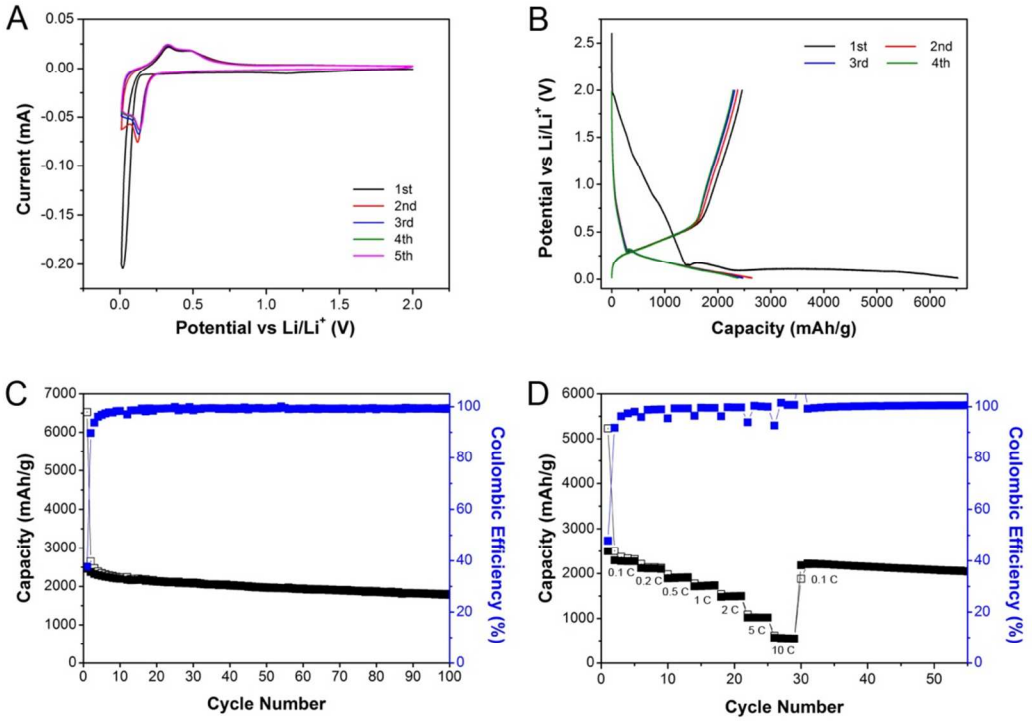

Fig. 4 Electrochemical performance of a battery using the 3D Si@Ni inverse opal structure as an anode within 0.01–2.0 V vs. Li/Li+. (A) Cyclic voltammetry curves of 3D Si@Ni inverse opal structure electrode for the first five cycles at a scan rate of 0.1 mV s-1. (B) Galvanostatic charge-discharge potential profiles for the first four cycles at 0.05 C rate (1 C = 4.2 A/g). (C) Specific capacity and coulombic efficiency vs. cycle number for 100 cycles at a rate of 0.05 C. (D) Specific capacity and coulombic efficiency vs. cycle number at 0.1 C, 0.2 C, 0.5 C, 1 C, 2 C, 5 C, and 10 C after the first cycle at 0.05 C.

the authors of that report measured the efficiency (η) of the Si electrodeposition to be approximately 35% (η = 0.35),[45] and others used this value to determine the mass and subsequent gravimetric capacity of electrodeposited Si.[33,46] However, we found that the efficiency of Si electrodeposition in our experimental system was *ca*. 74%, which was measured by using the moles of Si reduced following Faraday's law and measuring the exact mass of the electrodeposited Si with a microbalance for several samples. Based on the values we obtained, the first discharge capacity was 6524.9 mAh g^{-1}, with an irreversible loss of 62.3% (Fig. 4B). The unreasonably high discharge capacity and relatively high irreversibility of the capacity in the first cycle could be attributed to the possible side reactions of impurities and the formation of a solid electrolyte interface (SEI) layer on the Si surface.[31-33,47] The relatively high irreversible capacity loss in the first cycle could be reduced by introducing a thin layer of carbon on the Si surface, which would minimize the direct contact between the Si and the electrolyte and allow for stable formation of an SEI layer on the Si surface.[11,21,27] With subsequent cycles, the irreversible capacity loss dramatically decreased, indicating that possible side reactions occurred mostly in the first cycle and terminated in a few cycles.

The cycle performance of the 3D porous Si@Ni inverse opal structure anode at 0.05 C is shown in Fig. 4C. The first charge capacity was 2458.4 mAh g^{-1} with a coulombic efficiency of 37.7%, which was relatively low, but it rapidly increased to more than 98% in a few cycles. The charge capacity remained at 1772.7 mAh g^{-1} after 100 cycles, indicating a capacity retention of 72.1% and the capacity decrease per cycle was ~0.28%. The high cycle performance and coulombic efficiency of the 3D porous Si@Ni inverse opal structure anode can be attributed to several factors: *i*) The 3D porous inverse opal structure effectively accommodated volume changes of Si during discharging (Si–Li alloying), *ii*) the Ni scaffold inside the structure improved the electric conductivity of the electrode and the structural integrity, and *iii*) the large surface area of the conductive Ni scaffold, and thus the large contact area between Si and Ni, allowed uniform Li insertion and extraction within the Si.[31,32] In addition to these strengths of the 3D porous Si@Ni inverse opal structure, 3D interconnected pores within the structure allowed to be expect to exhibit high rate performance. Fig. 4D shows the rate performance of the 3D porous Si@Ni inverse opal structure anode, where the cell was cycled continuously at C rates of 0.05 C, 0.1 C, 0.2 C, 0.5 C, 1 C, 2 C, 5 C, and 10 C. The charge capacities gradually decreased from 2503.2 to 2295.0, 2119.7, 1902.0, 1729.0, 1493.9, and 1021.6 mAh g^{-1} as the C rate was increased from 0.05 C to 5 C, respectively. Even when the cell was cycled at 10 C, the charge capacity remained at 570.9 mAh g^{-1}, which is still higher than the theoretical charge capacity of graphite (372 mAh g^{-1}). The reduced charge capacity at higher C rates nearly recovered to 2206.2 mAh g^{-1} at a subsequent C rate of 0.1 C, which also indicates the high cycleability and rate capability of the prepared 3D porous Si@Ni inverse opal structure anode.

Conclusion

In summary, we have demonstrated that 3D porous Si@Ni inverse opal structures were successfully fabricated by using a simple, low-cost electrodeposition method. The highly porous structure of the electrode containing a conductive and mechanically strong Ni scaffold sufficiently accommodated the volume expansion during the Si–Li alloying. The resulting coin-type battery exhibited a high charge capacity of 2548.5 mAh g^{-1}, stable cycling retention, and high rate performance without the need for a binder or conducting additives. This fabrication route may be extended to fabricate metal-based electrodes for high-performance energy storage systems.

Acknowledgements

This work was financially supported by grants from the Fundamental R&D Program for Core Technology of Materials by the Ministry of Knowledge Economy and the Government-Funded General Research & Development Program by the Ministry of Trade, Industry and Energy, Republic of Korea.

Notes and references

[a] Advanced Materials Division, Korea Research Institute of Chemical Research, 141 Gajeong-ro, Yuseong-gu, Daejeon 305-600, Republic of Korea.

[b] Department of Chemical Engineering, College of Engineering, Kyung Hee University, Yongin-si, Kyunggi-do 446-701, Republic of Korea.

[c] Department of Chemical and Biomolecular Enginnering, KAIST, 291 Daehak-ro, Yuseong-gu, Daejeon 305-701, Republic of Korea.

† Electronic Supplementary Information (ESI) available: [XPS spectra of the Si@Ni inverse opal structure]. See DOI: 10.1039/b000000x/

1 J. R. Owen, *Chem. Soc. Rev.*, 1997, **26**, 259.
2 B. Scrosati, J. Garche, *J. Power Sources*, 2010, **195**, 2419.
3 H. Li, Z. X. Wang, L. Q. Chen, X. J. Huang, *Adv. Mater.*, 2009, **21**, 4593.
4 A. S. Arico, P. Bruce, B. Scrosati, J. M. Tarascon, W. Van Schalkwijk, *Nat. Mater.*, 2005, **4**, 366.
5 J. M. Tarascon, M. Armand, *Nature*, 2001, **414**, 359.
6 J. B. Goodenough, Y. Kim, *Chem. Mater.*, 2009, **22**, 587.
7 L. Zhang, G. Zhang, H. B. Wu, L. Yu, X. W. Lou, *Adv. Mater.*, 2013, **25**, 2589.
8 A. Magasinski, P. Dixon, B. Hertzberg, A. Kvit, J. Ayala, G. Yushin, *Nat. Mater.*, 2010, **9**, 353.
9 H. Zhang, X. Yu, P. V. Braun, *Nat. Nanotech.*, 2011, **6**, 277.

10 Y. Yao, K. Huo, L. Hu, N. Liu, J. J. Cha, M. T. McDowell, P. K. Chu, Y. Cui, *ACS Nano*, 2011, **5**, 8346.
11 S. Lee, Y. Cho, H.-K. Song, K. T. Lee, J. Cho, *Angew. Chem. Int. Ed.*, 2012, **51**, 1.
12 C. K. Chan, H. Peng, G. Liu, K. McIlwrath, X. F. Zhang, R. A. Huggins, Y. Cui, *Nat. Nanotech.*, 2008, **3**, 31.
13 L. Ji, H. Zheng, A. Ismach, Z. Tan, S. Xun, E. Lin, V. Battaglia, V. Srinivasan, Y. Zhang, *Nano energy*, 2012, **1**, 164.
14 L. Ji, Z. Lin, M. Alcoutlabi, X. Zhang, *Energy Environ. Sci.*, 2011, **4**, 2682.
15 X. W. Lou, L. A. Archer, Z. Yang, *Adv. Mater.*, 2008, **20**, 3987.
16 B. A. Boukamp, G. C. Lesh, R. A. Huggins, *J. Electrochem. Soc.*, 1981, **128**, 725.
17 Y. P. Wu, C. Y. Jiang, C. R. Wan, E. Tsuchida, *Electrochem. Commun.*, 2000, **2**, 272.
18 H. Wu, Y. Cui, *Nano Today*, 2012, **7**, 414.
19 R. Teki, M. K. Datta, R. Krishnan, T. C. Parker, T.-M. Lu, P. N. Kumta, N. Koratkar, *Small*, 2009, **5**, 2236.
20 J. R. Szcwech, S. Jin, *Energy Environ. Sci.*, 2011, **4**, 56.
21 M.-H. Park, M. G. Kim, J. Joo, K. Kim, J. Kim, S. Ahn, Y. Cui, J. Cho, *Nano Lett.*, 2009, **9**, 3844.
22 T. Song, J. Xia, J.-H. Lee, D. H. Lee, M.-S. Kwon, J.-M. Choi, J. Wu, S. K. Doo, H. Chang, W. I. Park, D. S. Zang, H. Kim, Y. Huang, K.-C. Hwang, J. A. Rogers, U. Paik, *Nano Lett.*, 2010, **10**, 1710.
23 L. F. Cui, R. Ruffo, C. K. Chan, H. Peng, Y. Cui, *Nano Lett.*, 2009, **9**, 491.
24 H. Kim, J. Cho, *Nano Lett.*, 2008, **8**, 3688.
25 R. Huang, X. Fan, W. Shen, J. Zhu, *Appl. Phys. Lett.*, 2009, **95**, 133119.
26 W. Wang, P. K. Kumta, *ACS Nano*, 2010, **4**, 2233.
27 B. M. Bang, J.-I. Lee, H. Kim, J. Cho, S. Park, *Adv. Energy Mater.*, 2012, **2**, 878.
28 M. Thakur, S. L. Sinsabaugh, M. J. Isaacson, M. S. Wong, S. L. Biswal, *Sci. Rep.*, 2012, **2**, 795.
29 J. Zhu, C. Gladden, N. Liu, Y. Cui, X. Zhang, *Phys. Chem. Chem. Phys.*, 2013, **15**, 440.
30 H. Kim, B. Han, J. Choo, J. Cho, *Angew. Chem. Int. Ed.*, 2008, **47**, 10151.
31 H. Zhang, P. V. Braun, *Nano Lett.*, 2012, **12**, 2778.
32 A. Esmanski, G. A. Ozin, *Adv. Func. Mater.* 2009, **19**, 1999.
33 X. Chen, K. Gerasopoulos, J. Cuo, A. Brown, C. Wang, R. Ghodssi, J. N. Culver, *Adv. Func. Mater.*, 2011, **21**, 380.
34 M. Paunovic, M. Schlesinger, *in Fundamentals of Electrochemical Deposition*, John Wiley & Sons, New Jersey, 2nd edn., 2006, ch. 1, pp.1-6.
35 E. C. Walter, M. P. Zach, F. Favier, B. J. Murray, K. Inazu, J. C. Hemminger, R. M. Penner, *ChemPhysChem*, 2003, **4**, 131.
36 L. P. Bicelli, B. Bozzini, C. Mele, L. D'Urzo, *Int. J. Electrochem. Sci.*, 2008, **3**, 356.
37 R. Winand, *Electrochem. Acta*, 1994, **39**, 1091.
38 N. Okamoto, F. Wang, T. Watanabe, *Mater. Trans.*, 2004, **45**, 3330.
39 J. Suk, D. Y. Kim, D. W. Kim, Y. Kang, *J. Mater. Chem. A*, 2014, **2**, 2487.
40 J. H. Kim, M. Chainey, M. S. El-Aasser, J. W. Vanderhoff, *J. Polym. Sci., Part A: Polym. Chem.*, 1992, **30**, 171.
41 H. K. Choi, S. H. Im, O O. Park, *Langmuir*, 2010, **26**, 12500.
42 K. Agrawal, A. E. Austin, *J. Electrochem. Soc.*, 1981, **128**, 2292.
43 J. P. Nicholson, *J. Electrochem. Soc.*, 2005, **152**, C795.
44 X. Yang, Z. Wen, X. Zhu, S. Huang, *Electrochem. Solid-State Lett.*, 2005, **8**, A481.
45 R. Epur, M. Ramanathan, F. R. Beck, A. Manivannan, P. N. Kumta, *Mater. Sci. Eng. B*, 2012, **177**, 1157.
46 J. Gobet, H. Tannenberger, *J. Electrochem. Soc.*, 1988, **135**, 109.
47 Y. M. Kim, J. Y. Lee, H.-T. Shim, K. K. Lee, J.-K. Park, *J. Electrochem. Soc.*, 2007, **154**, A515.

Table of Contents

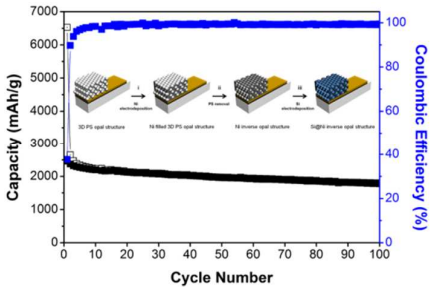

Si@Ni inverse opal structure fabricated by using an inexpensive elelctrodeposition method and a colloidal crystal template exhibits high capacity, cycleability, and rate-performance as an anode for Li ion battery.